Acta Oceanol. Sin., 2015, Vol. 34, No. 3, P. 31–41
DOI: 10.1007/s13131-015-0631-x
http://www.hyxb.org.cn
E-mail: hyxbe@263.net

Sea level rise projection in the South China Sea from CMIP5 models

HUANG Chuanjiang[1], QIAO Fangli[1]*

[1] Key Laboratory of Marine Science and Numerical Modeling, First Institute of Oceanography, State Oceanic Administration, Qingdao 266061, China

Received 25 May 2014; accepted 10 October 2014

Abstract

Future potential sea level change in the South China Sea (SCS) is estimated by using 24 CMIP5 models under different representative concentration pathway (RCP) scenarios. By the end of the 21st century (2081–2100 relative to 1986–2005), the multimodel ensemble mean dynamic sea level (DSL) is projected to rise 0.9, 1.6, and 1.1 cm under RCP2.6, RCP4.5, and RCP8.5 scenarios, respectively, resulting in a total sea level rise (SLR) of 40.9, 48.6, and 64.1 cm in the SCS. It indicates that the SCS will experience a substantial SLR over the 21st century, and the rise is only marginal larger than the global mean SLR. During the same period, the steric sea level (SSL) rise is estimated to be 6.7, 10.0, and 15.3 cm under the three scenarios, respectively, which accounts only for 16%, 21% and 24% of the total SLR in this region. The changes of the SSL in the SCS are almost out of phase with those of the DSL for the three scenarios. The central deep basin has a slightly weak DSL rise, but a strong SSL rise during the 21st century, compared with the north and southwest shelves.

Key words: sea level rise, South China Sea, dynamic sea level, steric sea level, CMIP5 models

Citation: Huang Chuanjiang, Qiao Fangli. 2015. Sea level rise projection in the South China Sea from CMIP5 models. Acta Oceanologica Sinica, 34(3): 31–41, doi: 10.1007/s13131-015-0631-x

1 Introduction

Sea level rise (SLR) has become apparent with global warming in recent decades. It has raised great concern as one of potentially socioeconomic hazards associated with the anthropogenic climate change. The global mean SLR is mainly induced by the thermal expansion of ocean water and the melting of land ice. The SLR in the global oceans has been extensively studied, whose results are usually inconsistent due to different data sets and time periods used. The recent IPCC fifth assessment report (AR5) estimated that the rate of the global mean SLR was about 1.7 mm/a for the 20th century, and increased to 3.2 mm/a for the period 1993–2010 (Rhein et al., 2013). This rise is expected to accelerate in the 21th century in response to the global warming. By the end of the 21st century (2081–2100), the global mean SLR is projected to reach a rate of 11.2 mm/a under the business-as-usual emission scenario (Church et al., 2013).

The SLR is highly nonuniform among ocean basins due to effects of wind and ocean circulation (Church et al., 2004; Beckley et al., 2010; Dong and Zhou, 2013). In some regions, local sea level changes can reach up to three times the global mean changes (Milne et al., 2009; Woodworth et al., 2011). The South China Sea (SCS) is the largest semienclosed marginal sea in the northwest Pacific Ocean, where the sea level has presented the significant change over recent decades, and this change deviates greatly from those in its adjacent and global oceans (Nidheesh et al., 2013). The rate of the SLR inferred from satellite altimetry data in the SCS is 10.3 mm/a for the period 1993–1999 (Li et al., 2002), 6.7 mm/a for 1993–2003 (Fang et al., 2006), and 5.5 mm/a for 1993–2009 (Feng et al., 2012), which all are significantly higher than the global mean rate for the same periods.

The SCS is significantly affected by the El Niño-Southern Oscillation (ENSO) (Rong et al., 2007; Wu et al., 2009a, b; Zhou et al., 2009). The altimetry-based data set mostly reflects interannual and decadal variations, rather than long-term trends because of its relatively short observational period. Recently, Peng et al. (2013) analyzed past sea level reconstruction data, and suggested that the rate of the SLR over the SCS is 1.7 mm/a during 1950–2009, which is almost consistent with the global mean rate.

However, these studies devoted extensively to the past SLR of the SCS, especially for the last two decades. Few efforts were paid to the projection of the sea level change in this area, although it is important to policymakers for coastal and insular planning in adapting to the climate change. Earth system models provide a tool for addressing this need. This study is attempted to project the future potential SLR in the SCS by using 24 CMIP5 models (the coupled model intercomparison project phase 5) (Taylor et al., 2012). The models and the methods used in this study are introduced in Section 2. We present the projections of the dynamic sea level (DSL) and the steric sea level (SSL) in the SCS during the 21st century in Section 3. The full SLR is estimated from a combination of the local DSL change and the global mean sea level change. We also evaluated the ability of CMIP5 models in simulating historical DSL and SSL changes in this section. The conclusion is given in Section 4.

2 Models and methods

2.1 *Models*

The 24 CMIP5 models from 15 scientific institutions are used

Foundation item: The National Basic Research Program (973 Program) of China under contract No. 2010CB950501; the National Natural Science Foundation of China under contract No. 41276035; the National Natural Science Foundation of China–Shandong Province Joint Fund of Marine Science Research Centers under contract No. U1406404.
*Corresponding author, E-mail: qiaofl@fio.org.cn

in this study (Table 1). The ocean component of these models uses different ocean general circulation models (OGCMs), and therefore differs greatly from each other in terms of model configurations (Flato et al., 2013; Huang, Qiao and Dai, 2014). In the 24 models, the volume-conserving Boussinesq scheme is used by 20 models; the mass-conserving non-Boussinesq scheme is used in the other four models (GISS-E2-R, GISS-E2-R-CC, NorESM1-M and NorESM1-ME). Non-Boussinesq models contain explicitly steric effects associated with changes in the seawater temperature and salinity, compared with Boussinesq models. However, the non-Boussinesq steric effect has little impact on the large-scale patterns of the sea level (Greatbatch, 1994; Griffies and Greatbatch, 2012). For a coarse resolution OGCM, the errors due to the Boussinesq approximation are at the noise level, and negligible with respect to other model uncertainties (Losch et al., 2004).

OGCMs in early times are usually formulated under the rigid lid approximation with a virtual salt flux at the ocean surface. However, there have only two models (CanESM2 and CSIRO-Mk3-6-0) using this approximation, and six models (CanESM2, CSIRO-Mk3-6-0, CCSM4, CESM1-BGC, NorESM1-M and NorESM1-ME) using a virtual salt flux. Other models employ a free surface scheme with explicit freshwater fluxes on the ocean surface (Table 1).

Several available models are excluded in this study because their DSL must be corrected if used (Yin, 2012). For example, the DSL in the MIROC5 and the GISS-E2-R needs to be converted to the effective DSL through including the water equivalent of the sea ice. For several other models, such as ACCESS1-3, CNRM-CM5, and HadGEM2-ES, global mean sea level outputs show statistically significant drifts. The drifts are associated with incomplete spin-up of model control runs (Gleckler et al., 2012) or imbalance in the water budget (Marsland et al., 2013), which can significantly influence the evaluation of the sea level change (Gleckler et al., 2012).

Three experiments forced by different representative concentration pathway (RCP) emission scenarios are used to project the SLR during the 21st century: the RCP4.5 is a stabilization scenario with the imposition of emissions mitigation policies to reduce the anthropogenic emissions leading to a radiative forcing of 4.5 W/m^2 in the year 2100; the RCP2.6 is a low scenario, in which the radiative forcing peaks at 3 W/m^2 and then declines to approximately 2.6 W/m^2 by 2100; while the RCP8.5 is a business-as-usual scenario, whose radiative forcing increases throughout the 21st century before reaching a level of about 8.5 W/m^2 in 2100 (Moss et al., 2010). In addition, the historical experiment is used to evaluate the ability of CMIP5 models in simulating the DSL and SSL changes. This experiment is the 20th century simulation forced by the observed atmospheric composition changes, including both natural and anthropogenic sources.

The model grids vary greatly among the model outputs (Flato et al., 2013; Huang, Qiao, Song, et al., 2014), and some of models implemented ensemble runs, which were initialized with slightly different conditions (Taylor et al., 2012). For simplicity, only monthly-averaged outputs with an ensemble number of *r1i1p1* were analyzed for each model, and all models outputs were regridded to a regular 1°×1° grid by the bilinear interpolation prior to analysis.

2.2 *Methods*

Although the performance of the CMIP5 models in simulating the sea level has been substantially improved compared with previous versions, these models do still not take into ac-

Table 1. CMIP5 model details

(Model number) Model name	Model ID	Historical	RCP2.6	RCP4.5	RCP8.5	Sea level representation (references)
(1) ACCESS1-0	CSIRO-BOM	D/S		D/S	D/S	BO, FS, FWF (Bi et al., 2013)
(2) BCC-CSM1-1	BCC-CMA	D/S	D/S	D/S	D/S	BO, FS, FWF (Griffies et al., 2005)
(3) BCC-CSM1-1-m		D/S	D/S	D/S	D/S	
(4) CanESM2	CCCMA	D/S	D/S	D/S	D	BO, RL, VSF (Merryfield et al., 2013)
(5) CCSM4	NCAR	D/S	D/S	D	D/S	BO, FS, VSF (Danabasoglu et al., 2012)
(6) CESM1-BGC	NSF-DOE-NCAR	D/S		D/S	D/S	
(7) CMCC-CM	CMCC	D/S		D/S	D/S	BO, FS, FWF (Fogli et al., 2009)
(8) CMCC-CMS		D/S		D/S	D/S	
(9) CSIRO-Mk3-6-0	CSIRO-QCCCE	D/S	D/S	D/S	D/S	BO, RL, VSF (Gordon et al., 2010)
(10) FGOALS-g2	LASG-CESS	D/S	D/S	D/S	D	BO, FS, FWF (Li et al., 2013)
(11) GFDL-CM3	NOAA-GFDL	D/S	D/S	D/S	D/S	BO, FS, FWF (Griffies et al., 2011)
(12) GFDL-ESM2G		D/S	D/S	D	D/S	BO, FS, FWF (Dunne et al., 2012)
(13) GFDL-ESM2M		D/S	D/S	D/S	D/S	
(14) GISS-E2-R	GISS-NASA	D/S	D/S	D/S	D	NB, FS, FWF (Liu et al., 2003)
(15) GISS-E2-R-CC		D/S		D/S	D	
(16) IPSL-CM5A-LR	IPSL	D/S	D/S	D/S	D	BO, FS, FWF (Dufresne et al., 2013)
(17) IPSL-CM5A-MR		D/S	D/S	D/S	D	
(18) IPSL-CM5B-LR		D/S		D/S	D	
(19) MIROC-ESM	MIROC	D/S	D	D/S	D	BO, FS, FWF (Watanable et al., 2011)
(20) MPI-ESM-LR	MPI-M	D/S	D/S	D/S	D/S	BO, FS, FWF (Jungclaus et al., 2013)
(21) MPI-ESM-MR		D/S	D/S	D	D/S	
(22) MRI-CGCM3	MRI	D/S	D/S	D/S	D	BO, FS, FWF (Yukimoto et al., 2012)
(23) NorESM1-M	NCC	D/S	D/S	D/S	D	NB, FS, VSF (Bentsen et al., 2012)
(24) NorESM1-ME		D/S	D/S	D/S	D	
Counts	15	24	18/17	24/21	24/11	

Notes: BO, Boussinesq; NB, non-Boussinesq; FS, free surface; RL, rigid lid; FWF, freshwater flux; and VSF, virtual salt flux. D and S present that DSL and SSL are available in this study, respectively.

count net ocean mass changes induced by melting glacies and ice sheets (Flato et al., 2013). Therefore, it is not possible to directly evaluate the real SLR. Instead, we analyze the DSL first, which is defined as the local sea level deviation from the global mean (Yin, 2012). The real SLR is estimated from a combination of the local DSL change and the global mean sea level change (Landerer et al., 2007). The DSL represents realistically the horizontal gradient of the sea level, and is closely related to surface winds and ocean currents. Its change can be explicitly and adequately simulated in current coupled general circulation models (Griffies and Greatbatch, 2012). The SSL is also analyzed, which represents the sea level change induced by the seawater temperature (thermosteric) and salinity (halosteric) variations throughout the water column.

In this study, the CMIP5 monthly output variable "zos" (i.e., sea surface height above geoid) is used to calculate the DSL. In some models, the global mean "zos" is not exactly 0 since the OGCM exchanges real freshwater with the other model components. Therefore a non-zero global mean is extracted prior to analysis. The SSL change, as well as its thermosteric and halosteric components (Landerer et al., 2007; Li et al., 2003), is calaulated as follows:

$$\Delta h_{\mathrm{s}} = \int_{-H}^{\eta} \frac{\rho(T_{\mathrm{c}}, S_{\mathrm{c}}, p) - \rho(T, S, p)}{\rho(T_{\mathrm{c}}, S_{\mathrm{c}}, p)} \mathrm{d}z, \tag{1}$$

$$\Delta h_{\mathrm{s}}^{\mathrm{ther}} = \int_{-H}^{\eta} \frac{\rho(T_{\mathrm{c}}, S_{\mathrm{c}}, p) - \rho(T, S_{\mathrm{c}}, p)}{\rho(T_{\mathrm{c}}, S_{\mathrm{c}}, p)} \mathrm{d}z, \tag{2}$$

$$\Delta h_{\mathrm{s}}^{\mathrm{halo}} = \int_{-H}^{\eta} \frac{\rho(T_{\mathrm{c}}, S_{\mathrm{c}}, p) - \rho(T_{\mathrm{c}}, S, p)}{\rho(T_{\mathrm{c}}, S_{\mathrm{c}}, p)} \mathrm{d}z, \tag{3}$$

where η is the free surface height; H is the water depth; T, S, p is the potential temperature, the salinity, and the pressure, respectively; and T_{c}, S_{c} are the climatological monthly temperature and salinity for the period 1986–2005 from the historical experiment. A modified UNESCO equation of state by Jackett and McDougall (1995) is used to calculate the density of sea water.

2.3 *Observed data*

In this study, the "observed" DSL is obtained from the monthly sea surface height data by Church et al. (2004), which were reconstructed from TOPEX/Poseidon satellite altimeter data and historical tide gauge data. This data set has a near-global coverage (between 65°S and 65°N) with a horizontal resolution of 1.0° and a span period of 1950–2001. In this data set, both inverse barometer correction and glacial isostatic adjustment correction were made, and seasonal signal was removed.

The "observed" SSL is calculated from monthly objectively analyzed subsurface temperature and salinity data developed by Ishii et al. (2006), which cover the global oceans with a horizontal resolution of 1.0°. An updated data set was used in this paper, which extended its end time from 2003 to 2012, and its depth from the upper 700 to 1 500 m.

3 Results

3.1 *Observations and simulations for historical DSL and SSL*

Figure 1 shows the observed and modeled historical sea level

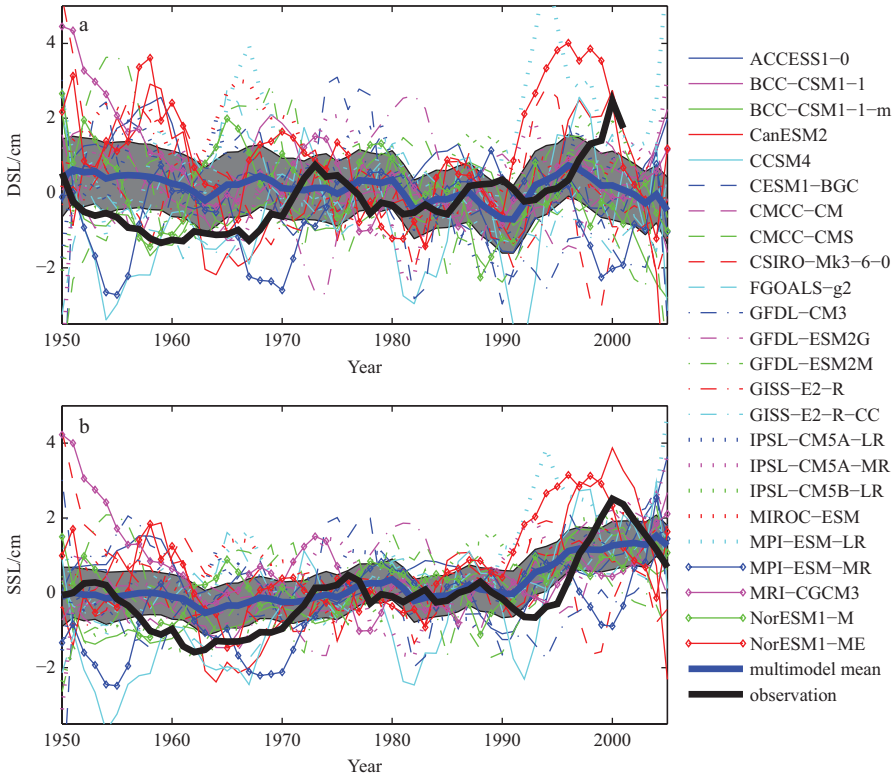

Fig. 1. Observed (thick black lines) and modelled DSL (a) and SSL (b) changes (multimodel means shown as thick blue lines, and 5%–95% confidence intervals shown as gray shadings) for the period 1950–2005 (relative to 1970–1989) in the SCS. A five-year running mean is applied to the time series.

changes in the SCS. The observed DSL experiences significantly decadal variation over past decades (Fig. 1). However, its change represents a near-zero trend from 1950 to the early 1990s, which indicates the sea level change in the SCS was consistent with the global mean change during this period. For the satellite altimetry era since 1993, however, the observed DSL rose rapidly during 1993–2000, while fell significantly in the following year. The observed SSL change bears a striking resemblance to the DSL change in the SCS (Fig. 1b). Their correlation coefficient can reach 0.71 during the period 1950–2001, which is statistically significant at the 95% confidence level.

This result agrees with the previous finding of Cheng and Qi (2007), which examined the 13 years merged satellite altimetry data, and found that the mean sea level over the SCS rose at a rate of 11.3 mm/a from 1993 to 2000, while fell at a rate of 11.8 mm/a from 2001 to 2005. This type of variation is related to decadal time-scale variability of the sea level, which can also be found in the previous observation, such as that from the late 1960s to the late 1970s. It indicates that the inferred SLR for the SCS is strongly dependent on the period of observations used, especially those for a relatively short time period (Li et al., 2002; Fang et al., 2006; Feng et al., 2012).

In general, the ensemble mean DSL and SSL from these models realistically reproduce the observed changes, in which most of observations are within a 5%–95% range of model results (Fig. 1). The consistence between the model and the observations is sufficient to encourage confidence in projecting the future sea level change using the models. Unfortunately, these models fail to simulate the low DSL and SSL during 1950–1970, as well as the high DSL and SSL around 2000. These extraordinary sea levels are believed to associate with the specific ENSO variability (Li et al., 2002; Peng et al., 2013), which is poorly simulated in current climate models (Flato et al., 2013).

In the 24 models, three Chinese models (BCC-CSM1-1, BCC-CSM1-1-m and FGOALS-g2) are included. Systematic assessments indicate that they all realistically reproduce many features of the climate system (e.g., Wu et al., 2010; Li et al., 2013). The first two models show a positive linear trend of 0.37 mm/a (BCC-CSM1-1) and 0.48 mm/a (BCC-CSM1-1-m) for the SSL during 1950–2005, respectively, which is close to the observation with a value of 0.37 mm/a. However, the FGOALS-g2 shows weak SSL rise, although it overestimates partly warming of global and regional surface air temperatures over past decades (Zhou et al., 2013). In this model, the trend of the SSL rise is only 0.17 mm/a. This weak trend is mainly caused by the false peak of the SSL in the 1960s (Fig. 1b).

3.2 *Future projection for DSL change*

The DSL changes over the SCS during the 21st century under the three RCP scenarios are examined in Fig. 2. Similar as those for the global ocean (Yin, 2012; Landerer et al., 2014), the projection of the DSL exhibits a considerable spread across these models in the SCS, especially that for RCP 8.5 (Fig. 2c). Bouttes and Gregory (2014) argued that this spread is mainly caused by to the spread in projected changes in the sea surface wind stress and heat fluxes.

Most of models simulate positive but very weak linear trends, in which the maximum is only 0.64 mm/a for the RCP2.6 (GFDL-CM3), 0.63 mm/a for the RCP4.5 (GFDL-ESM2M), and 1.04 mm/a for the RCP8.5 (NorESM1-M) during 2006–2100 (Fig. 3). In several other models, the projected DSL shows a negative trend in the 21st century. For the 24 models, the ensemble mean

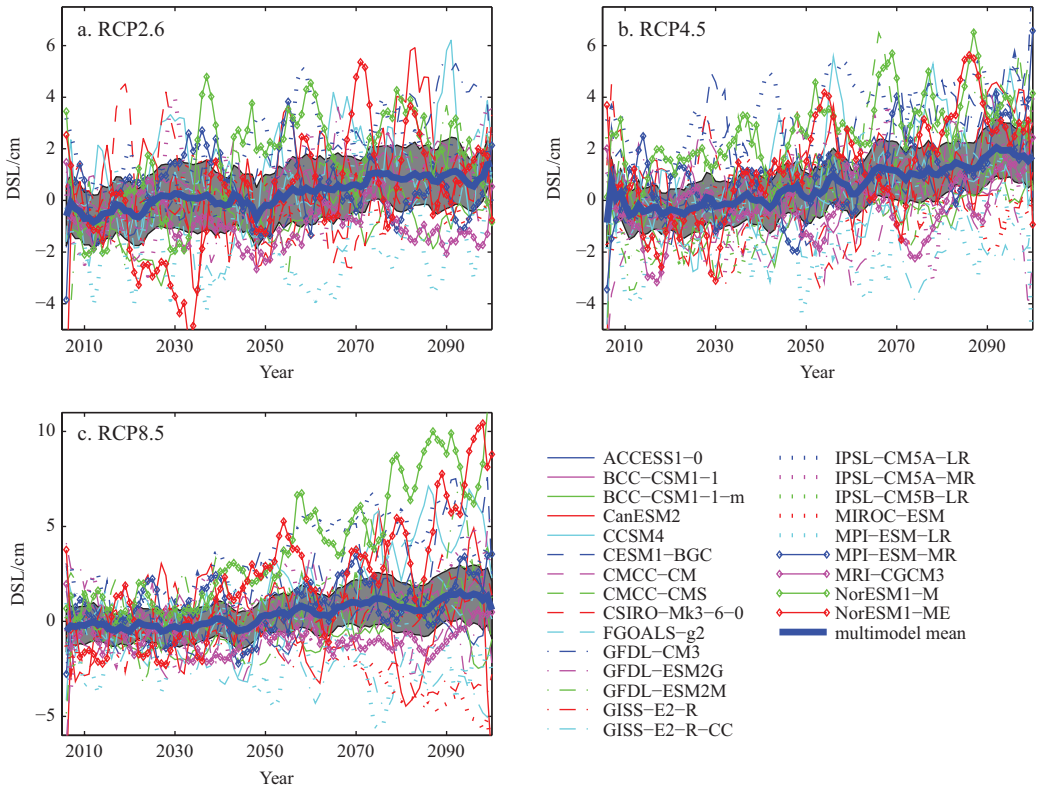

Fig. 2. Projections of DSL change (multimodel means shown as thick blue lines, and 5%–95% confidence intervals shown as gray shadings) in the SCS during the 21st century (relative to 1986–2005): RCP2.6 (a), RCP4.5 (b) and RCP8.5 (c) scenarios. A five-year running mean is applied to the time series.

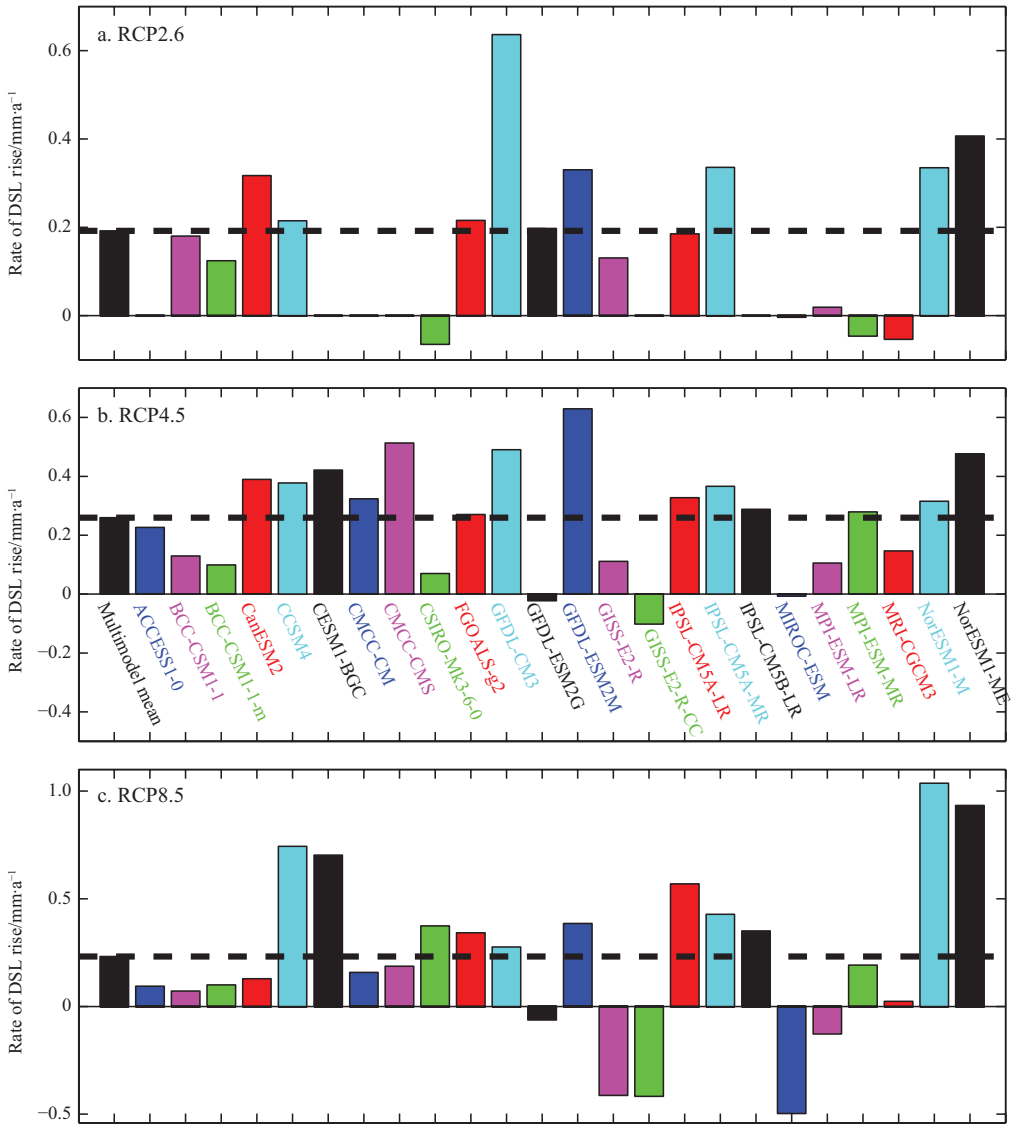

Fig. 3. Linear trend of DSL change in the SCS for the period 2006–2100: RCP2.6 (a), RCP4.5 (b) and RCP8.5 (c) scenarios. The dashed lines indicate values of multimodel ensemble.

DSLs rise at a rate of only 0.19, 0.26, and 0.23 mm/a under the RCP2.6, the RCP4.5, and the RCP8.5, respectively. This rise is not spatially uniform over the SCS, in which a somewhat large rise occurs in the north and southwest shelves of the basin (Fig. 4).

The full sea level change can be approximately obtained from superimposing the local DSL change on the global mean sea level change (Landerer et al., 2007), since the real sea level change still cannot be explicitly simulated from climate models (Church et al., 2013). The latter includes all the factors influencing the sea level changes, including thermal expansion, melting of glaciers and ice sheets, as well as land water storage. In the IPCC AR5, the glacier and ice-sheet contribution to sea level was calculated off-lined from the changes of the global mean surface air temperature, because the projections of glacier and ice-sheet volume changes still remain substantial uncertainties in current climate models. The sea level changes associated with melting glaciers and ice sheets have a complex pattern over the global oceans due to gravitational and loading effects on the sea level. Fortunately, their influence on the SCS is very close to the global mean, and large deviations mainly occur in the near field of the melt sources. The SLR over the SCS is estimated to be only about 1.1 mm/a if the global mean sea level resulting from melting of the Greenland or the West Antarctic ice sheets rises at a rate of 1 mm/a (Milne et al., 2009).

The IPCC AR5 analyzed 21 CMIP5 models with available projections of the surface air temperature and thermal expansion, and suggested that the global mean SLR by the end of the 21st century (2081–2100 relative to 1986–2005, the same below) can reach about 40 cm for the RCP2.6 scenario, 47 cm for the RCP4.5 scenario, and 63 cm for the RCP8.5 scenario (Church et al., 2013). However, the ensemble mean DSL rises in the SCS are only 0.9, 1.6, and 1.1 cm during this same period from the 24 models (Table 2), which is far smaller than those for the global mean. Therefore the SLR in the SCS is only marginally higher than that from the global mean during the 21th century. By the end of the 21th century, the total SLR in the SCS is expected to be 40.9, 48.6 and 64.1 cm under the three scenarios, with a 5%–95% uncertain range of 25.8–57.1, 32.6–65.6 and 44.7–84.5 cm.

This result is consistent with that from sea level reconstruction data over past decades, which is shown by Fig. 1a or Peng et

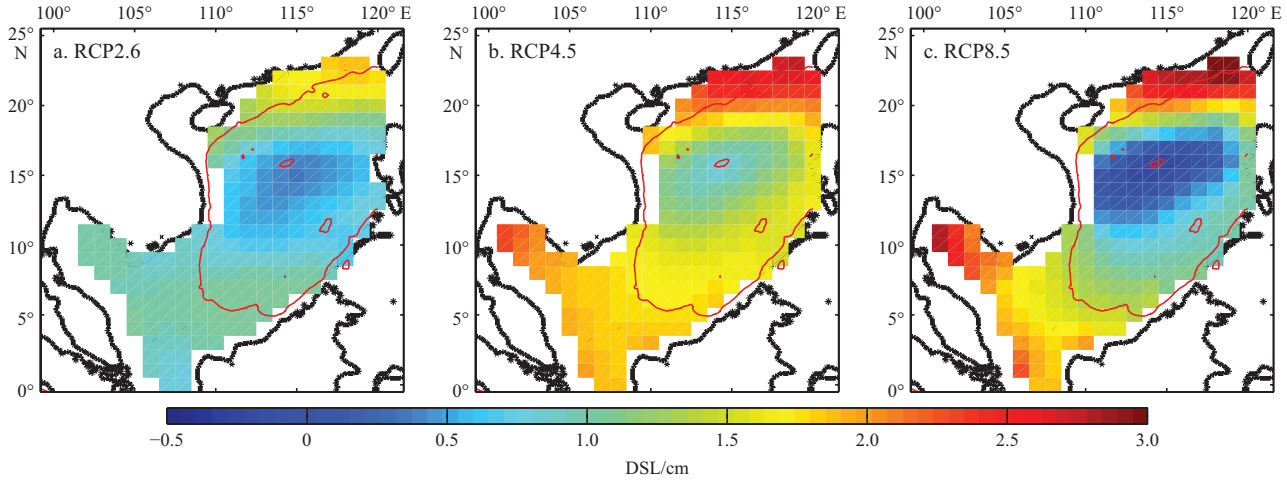

Fig. 4. The spatial distribution of projected ensemble mean DSL change in the SCS for the period 2081–2100 relative to 1986–2005. The red contours indicate the 200 m isobaths.

Table 2. Projected ensemble mean DSL and SSL rise in the SCS by 2081–2100 relative to 1986–2005 for the three RCP scenarios. The values in parentheses indicate the 5%–95% of confidence intervals.

	RCP2.6	RCP4.5	RCP8.5
DSL rise/cm	0.9 (−0.2–2.1)	1.6(0.6–2.6)	1.1(−0.3–2.5)
Total SLR[1)]/cm	40.9(25.8–57.1)	48.6(32.6–65.6)	64.1(44.7–84.5)
Thermosteric SLR/cm	4.8(4.0–5.6)	7.4(6.6–8.1)	10.9(9.3–12.5)
Halosteric SLR/cm	1.9(1.2–2.6)	2.6(1.9–3.4)	4.4(3.5–5.3)
Total SSL rise/cm	6.7(5.5–7.9)	10.0(8.9–11.1)	15.3(13.4–17.2)
Steric contributor/%	16	21	24
Global mean SLR/cm	40(26–55)	47(32–63)	63(45–82)

Notes: [1)] The total SLR in the SCS is obtained from superimposing the local DSL rise on the global mean SLR derived from Church et al. (2013).

al. (2013). Both of them suggest the long-term trend of the sea level change in the SCS just follows the global mean, instead of significant deviations inferred from satellite altimetry data since 1993 (e.g., Li et al., 2002; Fang et al., 2006; Feng et al., 2012). In fact, the strong DSL change appears mainly in the high-latitude and polar regions; in the tropical oceans including the SCS, the DSL changes is insignificant and then local SLRs are in roughly agreement with the global mean on centennial time scales (Yin et al., 2010; Yin, 2012). The IPCC AR5 also suggested that about 70% of the global coastlines will experience a relative sea level change with 20% of the global mean (Church et al., 2013).

3.3 *Future projection for SSL change*

The seawater temperature in the SCS is believed to be significantly warming in the 21st century, corresponding to the global warming. Huang, Qiao, Song, et al. (2014) projected the warming of the sea surface temperature in the SCS during the 21st century using 32 CMIP5 models, suggested that its linear trend is about 0.42, 1.50, and 3.30°C per century under the RCP2.6, RCP4.5 and RCP8.5 scenarios, respectively. This warming can rise the local sea level through the seawater thermal expansion.

Figure 5 shows projected the SSL changes over the SCS under the three scenarios, which all present strongly positive trends. Compared with the DSL (Fig. 2), the SSL has a relative weak intermodel spread. The RCP4.5 is a mid-range greenhouse gas emission scenario, in which the magnitude of the SSL change is between those of the RCP2.6 and the RCP8.5. For this scenario, the averaged trend of the SSL is estimated as 1.15 mm/a during the period 2006–2100 (Fig. 6), with a minimum of 0.73mm/a (FGOALS-g2) and a maximum of 1.73 mm/a (GFDL-CM3). The ensemble mean SSL rise is about 10.0 cm with a 5%–95% uncertain range from 8.9 to 11.1 cm by the end of the 21st century.

The RCP2.6 is a low emission scenario, while the RCP8.5 is a high emission scenario. Their SSL changes are similar as that in the RCP4.5, except with different magnitudes (Fig. 5). The ensemble mean SSL trend is only 0.71 mm/a in the RCP2.6 (Fig. 6a), compared with 1.87 mm/a in the RCP8.5 (Fig. 6c). By the end of the 21st century, their SSL rises amounts to 6.7 and 15.3 cm, respectively. The rises vary significantly with time. It is decelerating during the 21st century in the RCP2.6, which is in line with the peak of its radiative forcing around the mid-century and then declining (Moss et al., 2010). However, an accelerated rise occurs in the RCP8.5, reflecting its radiative forcing increasing throughout the century.

The halosteric effect is an important contribution to the future sea level change in the SCS (Fig. 7), although it is insignificant to the global mean sea level change. It-induced SLR amounts to 1.9, 2.6, and 4.4 cm by the end of the 21st century under the three scenarios (Table 2), respectively, which explain more than a quarter of the local SSL change. On the other hand, the thermosterically induced SLR is about 4.8, 7.4, and 10.9 cm during the same period (Fig. 8). The result confirms the conclusion that the SSL change in the marginal sea of China is mainly attributed to the thermosteric component (Dong and Zhou, 2013).

The changes of thermosteric and halosteric sea levels indi-

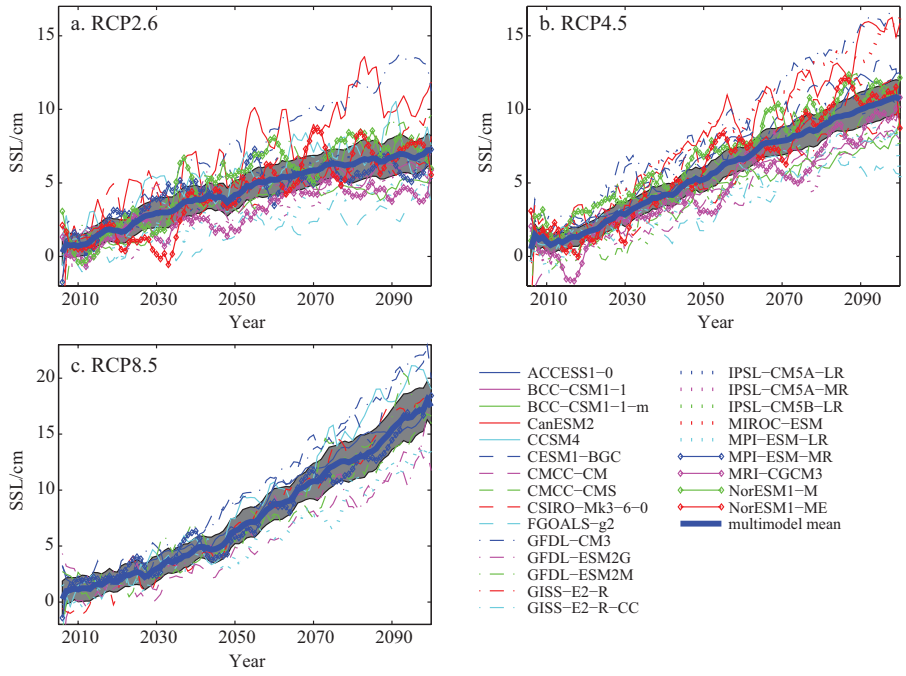

Fig. 5. Similar to Fig. 2, except for the SSL.

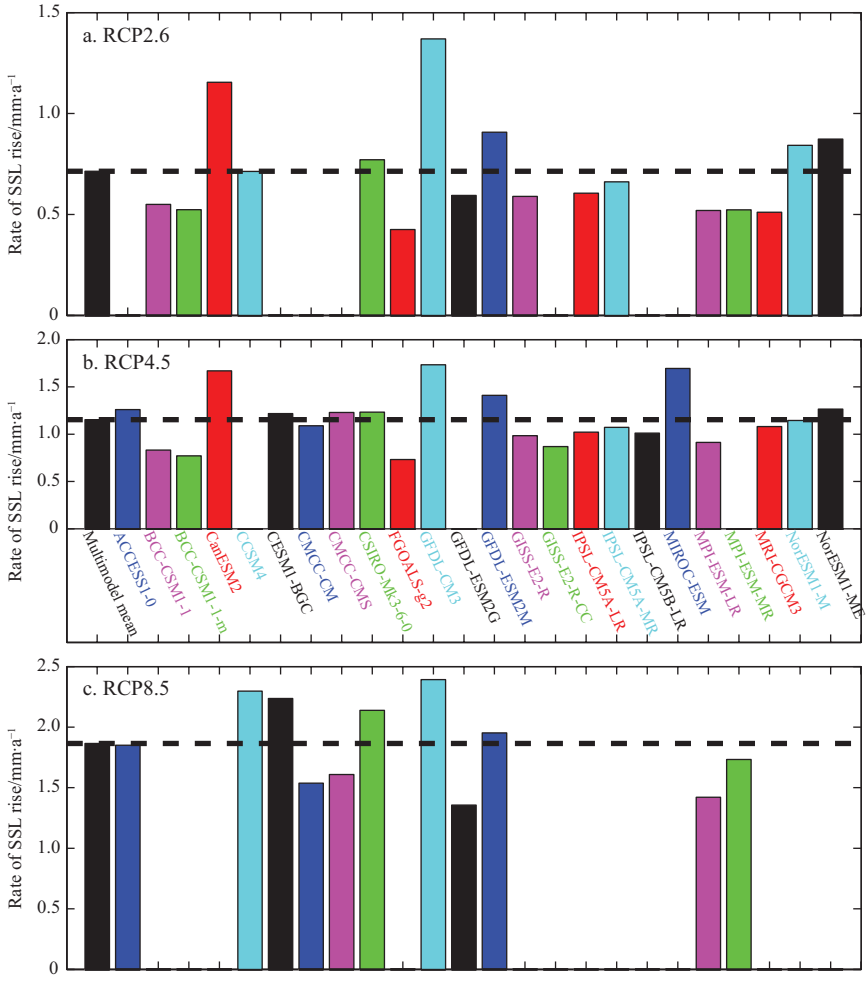

Fig. 6. Similar to Fig. 3, except for the SSL.

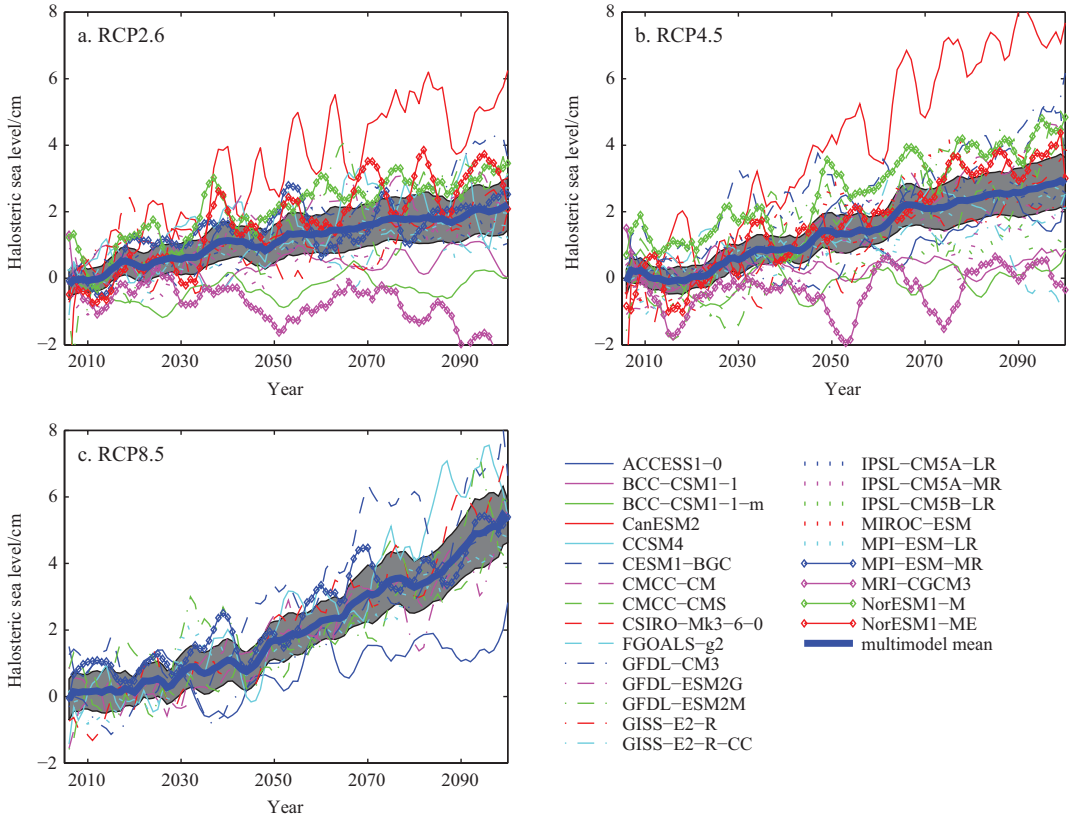

Fig. 7. Similar to Fig. 2, except for the halosteric sea level.

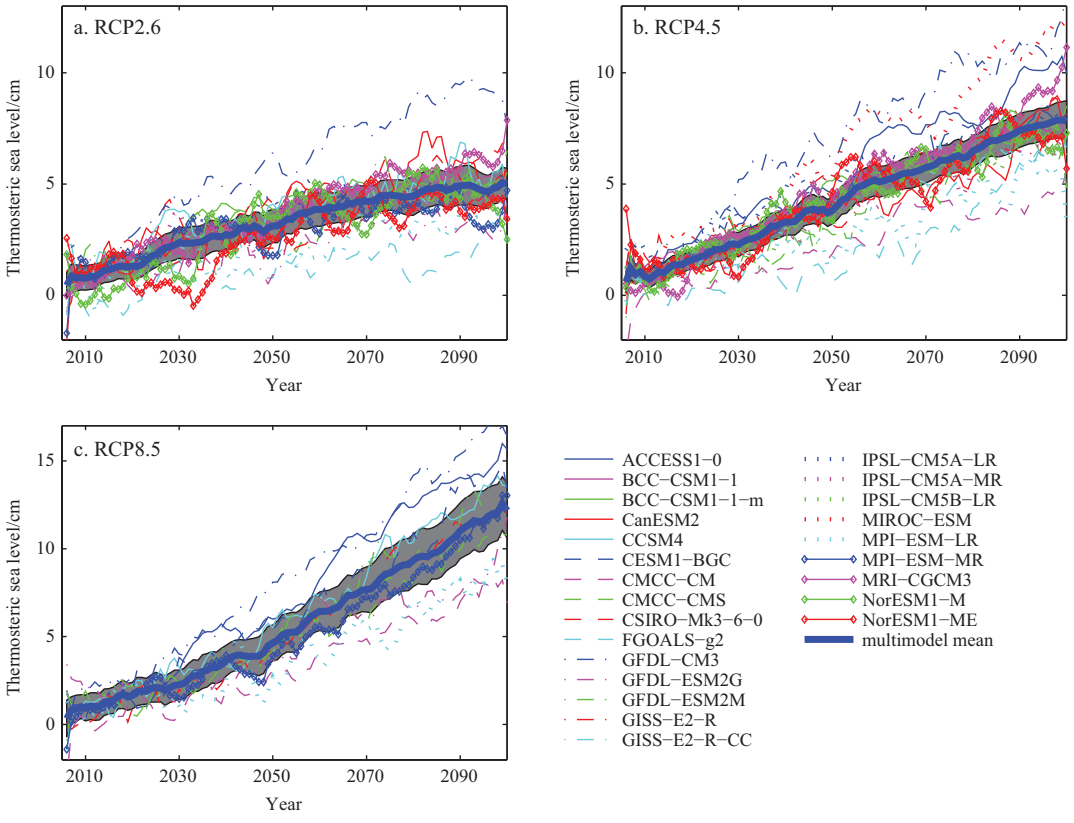

Fig. 8. Similar to Fig. 2, except for the thermosteric sea level.

cate that the SCS is significantly becoming warmer and fresher in the following century (Fig. 9). For example, the ensemble mean sea surface temperature can warm 2.85°C, and the sea surface salinity decreases 0.48 under the RCP8.5 scenario by the end of the 21st century. The changes are mainly located in the upper 1000 m. Under this depth, the changes of the seawater temperature and salinity are very weak, so that their contribution to the SSL changes is insignificant.

For the three scenarios, the ensemble mean SSL rise represents only 16%, 21% and 24% of the total sea level rise (see Table 2). It is well known that the steric effect is determined by seawater density changes throughout water depths. The SCS is a relatively shallow coastal sea, then the local steric effect is small in the long-term sea level change. The sea level changes associated with the seawater mass redistribution induced by land-ice melting and remote thermal expansion are more important relative to the local steric effect in this region.

Besides, the SSL change is also highly nonuniform among the ocean basins, and is almost out of phase with that of the DSL for the three scenarios (Fig. 10). In the deep basin of the central SCS deeper than 200 m, the local SSL rise is much higher than that in continental shelves. It can reach 14 cm for the RCP2.6 scenario, 20 cm for the RCP4.5 scenario, and 28 cm for the RCP8.5 scenario by the end of the 21st century. In the SCS, the significant anomalies of the seawater temperature and salinity can extend from the surface to 1000 m depth (Fig. 9), so the deep basin has a larger SSL change due to more heat uptake and more freshwater input. Nonuniform SSL changes can affect the horizontal pressure gradients of sea water, then currents through a geostrophic adjustment, which results in a redistribution of the seawater mass to the area with a weak SSL rise. Therefore the DSL in the shelves is slightly larger than that in the deep water.

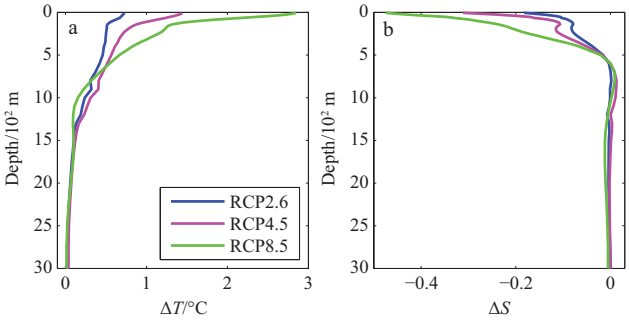

Fig. 9. Profiles of projected ensemble mean temperature (a) and salinity (b) changes in the SCS for the period 2081–2100 relative to 1986–2005.

4 Conclusions

In this study, we attempt to project the local sea level change in the SCS for the 21st century using 24 CMIP5 models. In general, the models can realistically reproduce the observed DSL and SSL changes over recent decades in this region, although they fail to simulate some interannual and decadal sea level fluctuations associated with the ENSO. The results show that the ensemble mean DSL rise by 2081–2100 relative to 1986–2005 in the SCS is about 0.9, 1.6, and 1.1 cm under the RCP2.6, RCP4.5 and RCP8.5 scenarios, respectively. As a result, its full SLR is estimated to be 40.9, 48.6, and 64.1 cm by the end of the 21st century under the three scenarios through combining the local DSL change with the global mean SLR. It indicates that the SCS is expected to experience a substantial SLR over the 21st century, but its rise is only marginal larger than the global mean SLR.

By the end of the 21st century, its SSL rise is projected to be 6.7, 10.0, and 15.3 cm under the RCP2.6, RCP4.5 and RCP8.5 scenarios, respectively, which represents only 16%, 21% and 24% of the total sea level rise. This implies that the rise in the SCS is dominated by the sea level changes associated with the seawater mass redistribution. The SSL change is highly nonuniform among the ocean basins, and is almost out of phase with that of the DSL for the three scenarios. The central deep basin has a slightly weak DSL rise, but a strong SSL rise compared with the north and southwest shelves.

It should be noted that although understanding and simulation on the sea level have significantly improved for the last decades, there are still considerable uncertainties in the projection of the sea level change, because the sea level reflects nearly all physical processes impacting the ocean (Griffies and Greatbatch, 2012). Providing the confident projection of global and regional sea level changes is more challenging because it is strongly dependent on accurate projections of other factors, such as the seawater temperature, salinity, circulation, precipitation and evaporation, ocean mass structure, as well as glaciers and ice sheets. Thus more efforts must be devoted due to its potential impacts for coastal society and economy.

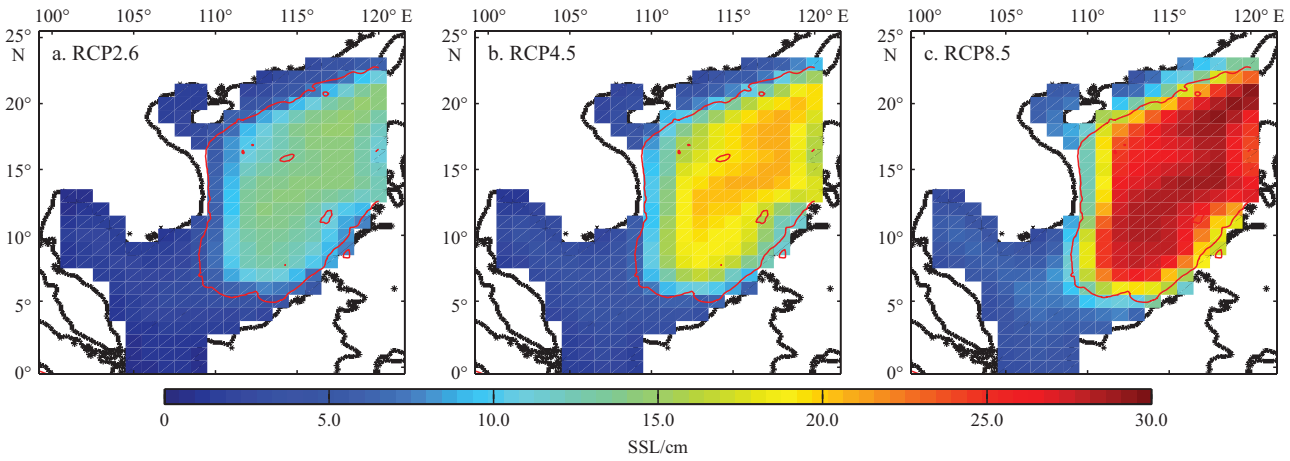

Fig. 10. Similar to Fig. 4, except for the SSL.

References

Beckley B D, Zelensky N P, Holmes S A, et al. 2010. Assessment of the Jason-2 extension to the TOPEX/Poseidon, Jason-1 sea-surface height time series for global mean sea level monitoring. Marine Geodesy, 33(1): 447–471

Bentsen M, Bethke I, Debernard J B, et al. 2012. The Norwegian earth system model, NorESM1-M: Part 1. description and basic evaluation. Geoscientific Model Development Discussions, 5: 2843–2931

Bi D, Dix M, Marsland S J, et al. 2013. The ACCESS coupled model: description, control climate and evaluation. Australian Meteorological and Oceanographic Journal, 63(1): 41–64

Bouttes N, Gregory J M. 2014. Attribution of the spatial pattern of CO_2-forced sea level change to ocean surface flux changes. Environmental Research Letters, 9(3): 034004

Cheng Xuhua, Qi Yiquan. 2007. Trends of sea level variations in the South China Sea from merged altimetry data. Global and Planetary Change, 57(3–4): 371–382

Church J A, Clark P U, Cazenave A, et al. 2013. Sea level change. In: Stocker T F, Qin D, Plattner G K, et al., eds. Climate Change 2013: The Physical Science Basis. Contribution of Working Group I to the Fifth Assessment Report of the Intergovernmental Panel on Climate Change. Cambridge: Cambridge University Press, 1137–1216

Church J A, White N J, Coleman R, et al. 2004. Estimates of the regional distribution of sea level rise over the 1950–2000 period. Journal of Climate, 17(13): 2609–2625

Danabasoglu G, Bates S C, Briegleb B P, et al. 2012. The CCSM4 ocean component. Journal of Climate, 25(5): 1361–1389

Dong Lu, Zhou Tianjun. 2013. Steric sea level change in twentieth century historical climate simulation and IPCC-RCP8. 5 scenario projection: a comparison of two versions of FGOALS model. Advances in Atmospheric Sciences, 30(3): 841–854

Dufresne J L, Foujols M A, Denvil S, et al. 2013. Climate change projections using the IPSL-CM5 earth system model: from CMIP3 to CMIP5. Climate Dynamics, 40(9–10): 2123–2165

Dunne J P, John J G, Adcroft A J, et al. 2012. GFDL's ESM2 global coupled climate-carbon earth system models: Part I. Physical formulation and baseline simulation characteristics. Journal of Climate, 25(19): 6646–6665

Fang Guohong, Chen Haiying, Wei Zexun, et al. 2006. Trends and interannual variability of the South China Sea surface winds, surface height, and surface temperature in the recent decade. Journal of Geophysical Research, 111(C11): C11S16

Feng Wei, Zhong Min, Xu Houze. 2012. Sea level variations in the South China Sea inferred from satellite gravity, altimetry, and oceanographic data. Science China: Earth Sciences, 55(10): 1696–1701

Flato G, Marotzke J, Abiodun B, et al. 2013. Evaluation of climate models. In: Stocker T F, Qin D, Plattner G K, et al., eds. Climate Change 2013: The Physical Science Basis. Contribution of Working Group I to the Fifth Assessment Report of the Intergovernmental Panel on Climate Change. Cambridge: Cambridge University Press, 741–866

Fogli P G, Manzini E, Vichi M, et al. 2009. INGV-CMCC carbon (ICC): a carbon cycle earth system model. In: CMCC Technical Reports. Lecce, Italy: Euro-Mediterranean Centre for Climate Change, 1–31

Gleckler P J, Santer B D, Domingues C M, et al. 2012. Human-induced global ocean warming on multidecadal time scales. Nature Climate Change, 2(7): 524–529

Gordon H, O'Farrell S, Collier M, et al. 2010. The CSIRO Mk3.5 Climate Model. CAWCR Technical Report No. 021. The Centre for Australian Weather and Climate Research, Melbourne, Victoria, Australia, 62. available online at: http://www.cawcr.gov.au/publications/technicalreports.php

Greatbatch R J. 1994. A note on the representation of steric sea level in models that conserve volume rather than mass. Journal of Geophysical Research, 99(C6): 12767–12771

Griffies S M, Gnanadesikan A, Dixon K W, et al. 2005. Formulation of an ocean model for global climate simulations. Ocean Science, 1: 45–79

Griffies S M, Greatbatch R J. 2012. Physical processes that impact the evolution of global mean sea level in ocean climate models. Ocean Modelling, 51: 37–72

Griffies S M, Winton M, Donner L J, et al. 2011. The GFDL CM3 coupled climate model: characteristics of the ocean and sea ice simulations. Journal of Climate, 24(13): 3520–3544

Huang Chuanjiang, Qiao Fangli, Dai Dejun. 2014. Evaluating CMIP5 simulations of mixed layer depth during summer. Journal of Geophysical Research: Oceans, 119(4): 2568–2582

Huang Chuanjiang, Qiao Fangli, Song Yajuan, et al. 2014. The simulation and forecast of SST in the South China Sea by CMIP5 models. Haiyang Xuebao (in Chinese), 36(1): 38–47

Ishii M, Kimoto M, Sakamoto K, et al. 2006. Steric sea level changes estimated from historical ocean subsurface temperature and salinity analyses. Journal of Oceanography, 62(2): 155–170

Jackett D R, McDougall T J. 1995. Minimal adjustment of hydrographic profiles to achieve static stability. Journal of Atmospheric and Oceanic Technology, 12(2): 381–389

Jungclaus J H, Fischer N, Haak H, et al. 2013. Characteristics of the ocean simulations in the Max Planck Institute ocean model (MPIOM) the ocean component of the MPI-Earth system model. Journal of Advances in Modeling Earth Systems, 5(2): 422–446

Landerer F W, Gleckler P J, Lee T. 2014. Evaluation of CMIP5 dynamic sea surface height multi-model simulations against satellite observations. Climate Dynamics, 43(5–6): 1271–1283

Landerer F W, Jungclaus J H, Marotzke J. 2007. Regional dynamic and steric sea level change in response to the IPCC-A1B scenario. Journal of Physical Oceanography, 37(2): 296–312

Li Lijuan, Lin Pengfei, Yu Yongqiang, et al. 2013. The flexible global ocean-atmosphere-land system model, grid-point version 2: FGOALS-g2. Advances in Atmospheric Sciences, 30(3): 543–560

Li Li, Xu Jindian, Cai Rongshuo. 2002. Trends of sea level rise in the South China Sea during the 1990s: an altimetry result. Chinese Science Bulletin, 47(7): 582–585

Li Wei, Zhang Xuehong, Jin Xiangze. 2003. Sea level height on different approximations assumptions in ocean circulation models. Advances in Marine Science (in Chinese), 21(2): 132–141

Liu Jiping, Schmidt G A, Martinson D G, et al. 2003. Sensitivity of sea ice to physical parameterizations in the GISS global climate model. Journal of Geophysical Research, 108(C2): 3053

Losch M, Adcroft A, Campin J M. 2004. How sensitive are coarse general circulation models to fundamental approximations in the equations of motion? Journal of Physical Oceanography, 34(1): 306–319

Marsland S J, Bi D, Uotila P, et al. 2013. Evaluation of ACCESS climate model ocean diagnostics in CMIP5 simulations. Australian Meteorological and Oceanographic Journal, 63(1): 101–119

Merryfield W J, Lee W S, Boer G J, et al. 2013. The Canadian seasonal to interannual prediction system: Part I. Models and initialization. Monthly Weather Review, 141(8): 2910–2945

Milne G A, Gehrels W R, Hughes C W, et al. 2009. Identifying the causes of sea-level change. Nature Geoscience, 2(7): 471–478

Moss R H, Edmonds J A, Hibbard K A, et al. 2010. The next generation of scenarios for climate change research and assessment. Nature, 463(7282): 747–756

Nidheesh A G, Lengaigne M, Vialard J, et al. 2013. Decadal and long-term sea level variability in the tropical Indo-Pacific Ocean. Climate Dynamics, 41(2): 381–402

Peng Dongju, Palanisamy H, Cazenave A, et al. 2013. Interannual sea level variations in the South China Sea over 1950–2009. Marine Geodesy, 36(2): 164–182

Rhein M, Rintoul S R, Aoki S, et al. 2013. Observations: ocean. In: Stocker T F, Qin D, Plattner G K, et al., eds. Climate Change 2013: The Physical Science Basis. Contribution of Working Group I to the Fifth Assessment Report of the Intergovernmental Panel on Climate Change. Cambridge: Cambridge University Press, 255–316

Rong Zengrui, Liu Yuguang, Zong Haibo, et al. 2007. Interannual sea level variability in the South China Sea and its response to ENSO. Global and Planetary Change, 55(4): 257–272

Taylor K E, Stouffer R J, Meehl G A. 2012. An overview of CMIP5 and the experiment design. Bulletin of the American Meteorological Society, 93(4): 485–498

Watanabe S, Hajima T, Sudo K, et al. 2011. MIROC-ESM: model de-

scription and basic results of CMIP5-20c3m experiments. Geoscientific Model Development Discussions, 4: 1063–1128

Woodworth P L, Gehrels W R, Nerem R S. 2011. Nineteenth and twentieth century changes in sea level. Oceanography, 24(2): 80–93

Wu Tongwen, Yu Rucong, Zhang Fang, et al. 2010. The Beijing Climate Center atmospheric general circulation model: description and its performance for the present-day climate. Climate Dynamics, 34(1): 123–147

Wu Bo, Zhou Tianjun, Li Tim. 2009a. Seasonally evolving dominant interannual variability modes of East Asian climate. Journal of Climate, 22(11): 2992–3005

Wu Bo, Zhou Tianjun, Li Tim. 2009b. Contrast of rainfall-SST relationships in the Western North Pacific between the ENSO-developing and ENSO-decaying summers. Journal of Climate, 22(16): 4398–4405

Yin Jianjun. 2012. Century to multi-century sea level rise projections from CMIP5 models. Geophysical Research Letters, 39(17): L17709

Yin Jianjun, Griffies S M, Stouffer R J. 2010. Spatial variability of sea level rise in twenty-first century projections. Journal of Climate, 23(17): 4585–4607

Yukimoto S, Adachi Y, Hosaka M, et al. 2012. A new global climate model of the Meteorological Research Institute: MRI-CGCM3-model description and basic performance. Journal of the Meteorological Society of Japan, 90A: 23–64

Zhou Tianjun, Song Fengfei, Chen Xiaolong. 2013. Historical evolution of global and regional surface air temperature simulated by FGOALS-s2 and FGOALS-g2: How reliable are the model results? Advances in Atmospheric Sciences, 30(3): 638–657

Zhou Tianjun, Wu Bo, Wang Bin. 2009. How well do atmospheric general circulation models capture the leading modes of the interannual variability of the Asian-Australian monsoon? Journal of Climate, 22(5): 1159–1173